

## Is the quark gluon plasma produced in RHIC collisions strongly coupled?

Roy A. Lacey<sup>1</sup>, Arkadij Taranenko<sup>1</sup> and Rui Wei<sup>1</sup>

<sup>1</sup> Chemistry Dept., Stony Brook University  
Stony Brook NY 11794-3400, USA

**Abstract.** Recent hexadecapole ( $v_4$ ) and elliptic ( $v_2$ ) flow measurements are used to constrain estimates for the degree of local equilibrium, mean free path  $\lambda$ , and the viscosity to entropy density ratio ( $\frac{\eta}{s}$ ) of the plasma produced in Au+Au collisions at  $\sqrt{s_{NN}} = 200$  GeV. The eccentricity-scaled flow coefficients  $\frac{v_2}{\varepsilon_2}$  and  $\frac{v_4}{\varepsilon_4}$  indicate that the plasma achieves a degree of local equilibrium within  $\sim 5 - 10\%$  of the value expected for a fluid with  $\frac{\eta}{s}$  equal to the conjectured lower bound of  $1/4\pi$ . Estimates for  $\lambda$  and  $\frac{\eta}{s}$  as a function of collision centrality and particle transverse momentum  $p_T$ , points to transverse expansion dynamics compatible with a strongly coupled low viscosity plasma.

*Keywords:* elliptic flow, hexadecapole flow, viscosity, mean free path, local equilibrium

*PACS:* 25.75.Dw, 25.75.Ld

### 1. Introduction

In central and mid-central Au+Au collisions at the Relativistic Heavy ion Collider (RHIC), matter is produced at energy densities well in excess of the value ( $\sim 1$  GeV/fm<sup>3</sup>) required for a de-confinement transition to the quark gluon plasma (QGP). A strong indication that such a de-confinement transition indeed occurs, is the important role that quark-like degrees of freedom have been found to play in the transverse expansion dynamics leading to anisotropic flow. Such flow is routinely characterized by the even order Fourier coefficients

$$v_n = \left\langle e^{in(\phi_p - \Phi_{RP})} \right\rangle, \quad n = 2, 4, \dots,$$

where,  $\phi_p$  is the azimuthal angle of an emitted particle,  $\Phi_{RP}$  is the azimuth of the reaction plane and the brackets denote averaging over particles and events. The second ( $v_2$ ) and fourth ( $v_4$ ) order coefficients characterize the magnitude of elliptic

and hexadecapole flow respectively.

At the highest RHIC collision energy of  $\sqrt{s_{NN}} = 200$  GeV, a universal scaling of elliptic flow, suggestive of constituent quark-like degrees of freedom in the collision zone, has been discovered [ 1, 2] and is now well established for a broad range of collision centralities, particle species and transverse kinetic energies. For transverse momenta  $p_T \lesssim 1.5$  GeV/c, hydrodynamic calculations that model a locally equilibrated QGP (with little or no viscosity) show good agreement with the data [ 3, 4, 5]. A recent transport calculation which incorporates gluon dynamics [ 6], also indicate good agreement with the magnitude and trend of centrality dependent  $v_2$  data. Thus, the measurement and study of flow have been central to the confluence of experimental results which now bear evidence for the creation of the QGP in heavy ion collisions at RHIC.

A less settled question which is still debated intensely, is the degree to which the QGP is thermalized [ 7], and whether it is strongly or weakly coupled [ 4, 8]. Experimental constraints which allow estimates of the ratio of viscosity to entropy density  $\frac{\eta}{s}$  and the mean free path  $\lambda$ , are crucial ingredients to the resolution of this question. In this contribution we show that the combined use of double differential  $v_2$  and  $v_4$  measurements provide such constraints, and consequently, lend new and important insight to this question.

## 2. Flow, local equilibrium & the coupling strength of the QGP

The use of flow correlations as a probe for the nuclear equation of state (EOS) and the transport coefficients of hot and dense nuclear matter has been recognized for quite some time [ 9, 10, 11, 12]. The connection is made transparent in the framework of perfect fluid hydrodynamics where the conceptual link between the conservation laws (baryon number, and energy and momentum currents) and the fundamental properties of a fluid (its equation of state and transport coefficients) is straightforward. Much current effort to understand and determine transport properties are focused on several microscopic models (for recent reviews see for example Refs. [ 4, 13]). Hybrid approaches which involve the parametrization of deviations from hydrodynamic behavior (i.e full local equilibrium) are currently being studied as well [ 14, 15, 16]. The latter exploits the fact that results from the Boltzmann equation reduce to those from perfect fluid hydrodynamics when the mean free path  $\lambda$  becomes small [ 17].

### 2.1. Deviation from local equilibrium

Further insight on the extent to which a system deviates from full local equilibrium can be obtained via simultaneous study of the scaling violations of  $v_2$  and  $v_4$ . Here, the central idea is that partial equilibrium breaks the scale invariance of perfect fluid hydrodynamics (which requires full local equilibrium), and thus, gives rise to specific measurable scaling violations [ 14, 15, 18]. The quantification of such

scaling violations can then be used to constrain an estimate of the “degree” of local equilibrium and the transport coefficients.

One such violation of the eccentricity-scaled second harmonic  $v_2/\varepsilon_2$ , has been recently parametrized [ 14, 15] via the Knudsen number  $K = \lambda/\bar{R}$  [ 19], as;

$$\frac{v_2}{\varepsilon_2} = \frac{v_2^h}{\varepsilon_2} \frac{K^{-1}}{K^{-1} + K_0^{-1}}, \quad (1)$$

where  $K^{-1}$  is proportional to the average number of collisions per particle  $N$ , in the collision zone of mean transverse size  $\bar{R}$ ;  $\lambda$  is the mean free path of these particles;  $\frac{v_2^h}{\varepsilon_2}$  is the eccentricity-scaled flow harmonic expected from perfect fluid hydrodynamics and  $K_0$  is a constant estimated to be  $0.7 \pm 0.03$  with the aid of a transport model [ 16]. We have found that a modified form of Eq. 1;

$$\frac{v_{2k}}{\varepsilon_{2k}} = \frac{v_{2k}^h}{\varepsilon_{2k}} \left[ \frac{K^{-1}}{K^{-1} + K_0^{-1}} \right]^k \quad k = 1, 2, \dots, \quad (2)$$

provides a good estimate of the scaling violations for all even order harmonics investigated.

Following the operational ansatz of Eq. 2, an estimate of the extent of the deviation from local equilibrium (degree of local equilibrium) can be obtained for a given centrality cut as:

$$\left( \frac{v_{2k}}{v_{2k}^h} \right)^{1/k} = \frac{1}{(1 + K/K_0)} \quad k = 1, 2, \dots,$$

where  $K$  is obtained as a function of centrality via a fit to the eccentricity-scaled flow coefficients, as discussed below.

## 2.2. Coupling strength and the ratio of viscosity to entropy density

The shear viscosity  $\eta$  of the QGP medium reflects its ability to flow “freely” locally. This medium response to flow gradients is proportional to the range over which momentum can be readily transported transverse to the flow. Consequently, a necessary indication for a strongly coupled QGP would be the observation of a rather small value for the ratio of viscosity to entropy density  $\eta/s$ . Here, it is noteworthy that this is a necessary but insufficient requirement because a weakly coupled system exhibiting anomalous viscosity could also give a relatively small  $\eta/s$  value [ 8]. The ratio  $\eta/s$ , of course, can not be arbitrarily small [ 20, 21] because quantum mechanics limits the size of cross sections via unitarity. Therefore, operationally it is the extraction of a relatively small  $\eta/s$  value in concert with a short mean free path ( $\lambda$ ), from data, that provides a robust indicator of a strongly coupled QGP.

For a relativistic fluid, the ratio of viscosity to entropy density can be estimated as:

$$\frac{\eta}{s} \approx T\lambda c_s \equiv K\bar{R}Tc_s, \quad (3)$$

where  $T$  and  $c_s$  are the temperature and speed of sound respectively. Thus, the  $K$  values extracted from fits to eccentricity-scaled flow data, taken in concert with an estimate of  $T$  and a reliable EOS, can be used to evaluate  $\frac{\eta}{s}$ . Similarly, the mean free path  $\lambda = K\bar{R}$ , can be estimated with the aid of the centrality dependent geometric value  $\bar{R}$ .

### 3. Proofing the extraction of Knudsen numbers from fits

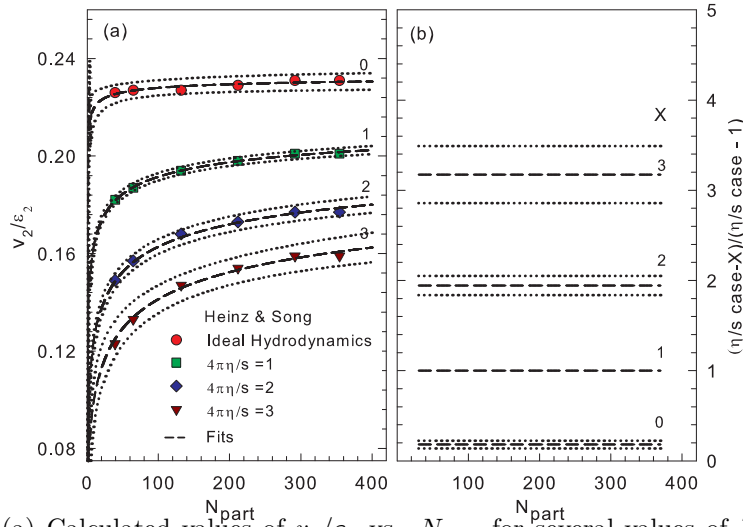


**Fig. 1.** (a) Calculated values of  $v_2/\epsilon_2$  vs.  $N_{part}$  for several values of  $\frac{\eta}{s}$  [18] as indicated. The dashed curves show the fits to these simulated data. (b)  $(\frac{\eta}{s}(\text{case} - 0, 1, 2, 3))/(\frac{\eta}{s}(\text{case} - 1))$  vs.  $N_{part}$  for the fits performed in panel (a) see text. The dotted curves represent error bands.

Reliable estimates for  $\frac{\eta}{s}$ ,  $\lambda$  and the degree of local equilibrium crucially depend on accurate extractions of the Knudsen number  $K$ , from fits to eccentricity-scaled flow data. Therefore, it is important to test the efficacy of the extraction procedure. Such a test is illustrated in Fig. 1 where we have performed fits to the eccentricity-scaled elliptic flow values  $\frac{v_2}{\epsilon_2}$ , recently calculated by Song and Heinz [18]. The symbols in Fig.1(a) show the  $\frac{v_2}{\epsilon_2}$  values obtained from hydrodynamic calculations performed for  $4\pi(\frac{\eta}{s})$  values of 0, 1, 2 and 3 respectively (hereafter referred to as *case* = 0, 1, 2, and 3 respectively). The dashed lines show the corresponding fits obtained with Eq. 2 and the assumption [14, 22] that

$$K^{-1} = \frac{\alpha}{S} \frac{dN}{dy} \sim \beta N_{part}^{1/3}$$

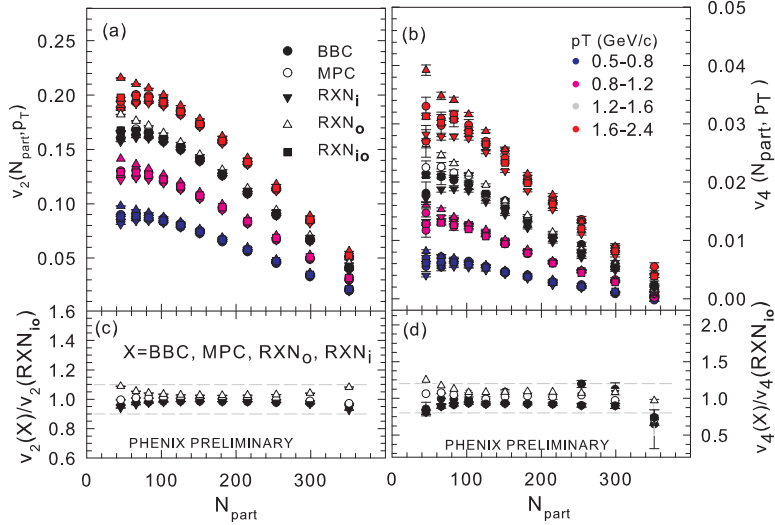


**Fig. 2.** (a)  $v_2$  vs.  $N_{part}$  and (b)  $v_4$  vs.  $N_{part}$  for charged hadrons obtained with several reaction plane detectors for the  $p_T$  selections indicated. The dashed lines in (c) and (d) show 10% and 20% error bands respectively.

where  $\alpha$  or  $\beta$  are fit parameters,  $S$  is the area of the collision zone,  $\frac{dN}{dy}$  is the multiplicity density and  $N_{part}$  is the number of participants.

The curves in Fig.1(a) indicate a good fit to the simulated data for each *case*. We reiterate here that the two parameters of the fit are the scaled hydrodynamic limit  $\frac{v_2^h}{\varepsilon_2}$  and  $\beta$ . The latter allows the determination of  $K$  for each centrality or value of  $N_{part}$ . For each fit indicated in Fig.1(a), the value of  $\frac{v_2^h}{\varepsilon_2}$  is within 5% of the calculated value of 0.23 (cf. solid circles in Fig.1). The dashed lines in Fig.1(b) show the ratio  $(\frac{v_2}{s}(case - 0, 1, 2, 3))/(\frac{v_2}{s}(case - 1))$  determined with Eq. 3 and the  $K$  values obtained from the extracted values of  $\beta$ . Within errors, the ratios shown in Fig. 1(b) are the same as the ratios of the  $\frac{v_2}{s}$  values employed in the hydrodynamic calculations. Therefore, we interpret this agreement to be a good validation test of the reliability of the the extraction technique.

#### 4. Flow measurements and their scaling violations

Reliable estimates for  $\frac{v_2}{s}$ ,  $\lambda$  and the degree of local equilibrium also demand robust measurements of the flow coefficients. Such measurements of  $v_2$  and  $v_4$  for charged hadrons produced in Au+Au collisions at  $\sqrt{s_{NN}} = 200$  GeV, have been recently carried out by the PHENIX collaboration. Fig. 2 shows a set of preliminary double

differential  $v_2$  and  $v_4$  data obtained from  $\sim 3.4 \times 10^9$  minimum-bias Au+Au events collected during the 2007 running period. These data were obtained via the reaction plane method of analysis [ 23];

$$v_{2k} = \frac{\langle \cos(2k(\varphi_p - \Phi_2)) \rangle}{\langle \cos(2k(\Phi_2 - \Phi_{RP})) \rangle} \quad k = 1, 2, \quad (4)$$

where,  $\varphi_p$  is the azimuthal angle of a charged track and  $\Phi_2$  is the azimuth of the estimated second order reaction (event) plane. Five separate event planes were constructed with the aid of the PHENIX Beam-Beam Counters (BBC:  $3.1 < |\eta_{BBC}| < 3.9$ ), Muon Piston Calorimeters (MPC:  $3.1 < |\eta_{MPC}| < 3.9$ ), and the inner (i:  $1.5 < |\eta_{RXN_i}| < 2.8$ ), outer (o:  $1.0 < |\eta_{RXN_o}| < 1.5$ ) and combined (io) rings (North and South) of the newly installed PHENIX reaction plane detectors (RXN).

The denominator of Eq. 4 is a resolution factor which corrects for the difference between the estimated  $\Phi_2$  and the true azimuth  $\Phi_{RP}$  of the reaction plane [ 23]. The three sub-event method [ 24] was employed to obtain an estimate of this resolution factor (as a function of centrality) for each of the five event planes used in our analysis. For  $k = 1$ , the resolution factor for the combined reaction plane from both BBC's has an average of 0.33 over centrality, with a maximum  $\approx 0.42$  in mid-central collisions [ 23, 1]. The MPC and  $RXN_{io}$  improve this resolution factor by about 35% and 100%, respectively.

For mid-central collisions, a comparison of the double differential flow coefficients  $v_{2,4}(p_T, N_{\text{part}})$ , shown for each event plane in Figs. 2(a) and (b), indicate excellent agreement (i.e much better than 5% and 10% for  $v_2$  and  $v_4$  respectively) over the broad range of  $p_T$  selections shown. For very central and peripheral collisions, this agreement degrades to  $\sim 10\%$  and  $20\%$  respectively. Here, it is important to note that; (i) the  $v_4$  signal is rather small (especially for low  $p_T$  and central collisions) and is very difficult to measure precisely with a poor reaction plane resolution. (ii) The event plane resolution, for each event plane detector, achieves a maximum in mid-central collisions and worsens as one moves towards central and peripheral collisions.

The rather good agreement between the measurements shown in Fig. 2 attests to their reliability and to the absence of a significant  $\eta$ -dependent non-flow contribution. A prodigious non-flow contribution, such as from di-jets, would lead to a sizable difference in the  $v_2$  values obtained with event planes determined at different rapidity gaps ( $\Delta\eta$ ) with respect to the central arms [ 25].

#### 4.1. Hydrodynamic scaling violations of $v_2$ and $v_4$

To test for hydrodynamic scaling violations in the data, we divide the  $v_2$  and  $v_4$  measurements obtained with the  $RXN_{io}$  event plane<sup>1</sup> (cf. Fig. 2), by the respective eccentricity (ie.  $\varepsilon_2$  and  $\varepsilon_4$ ) for each centrality selection. Here, the guiding principle is the prediction from perfect fluid hydrodynamics that  $v_{2,4}$  is proportional to the

<sup>1</sup>The  $RXN_{io}$  event plane detector provides an optimal resolution across collision centralities.

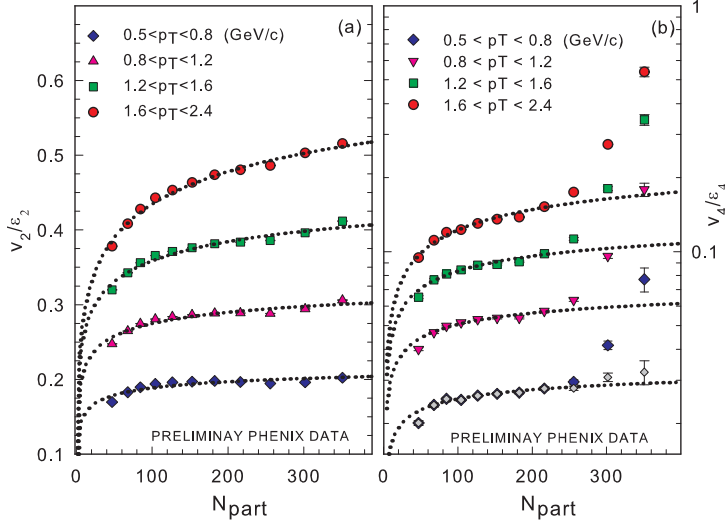


**Fig. 3.** (a)  $v_2/\varepsilon_2$  vs.  $N_{\text{part}}$  and (b)  $v_4/\varepsilon_4$  vs.  $N_{\text{part}}$  for several  $p_T$  selections as indicated. The dotted curves are fits to the data with Eq.2.

initial spatial eccentricity  $\varepsilon_{2,4}$  and is independent of the size of the collision zone  $\bar{R}$ . Thus, perfect eccentricity scaling would be indicated by a flat dependence for both  $\frac{v_2}{\varepsilon_2}$  and  $\frac{v_4}{\varepsilon_4}$  vs.  $N_{\text{part}}$ .

For each centrality selection, the number of participant nucleons  $N_{\text{part}}$ , was estimated via a Glauber-based model [26]. The corresponding transverse size  $\bar{R}$  and  $\varepsilon_{2,4}$  were estimated from the distribution of these nucleons in the transverse  $(x, y)$  plane via this same Monte-Carlo Glauber model [26, 27], as well as via the factorized Kharzeev-Levin-Nardi (fKLN) [28] model:

$$\frac{1}{\bar{R}} = \sqrt{\left(\frac{1}{\sigma_x^2} + \frac{1}{\sigma_y^2}\right)}, \varepsilon_2 = \frac{\sqrt{(\sigma_y^2 - \sigma_x^2)^2 + 4\sigma_{xy}^2}}{\sigma_x^2 + \sigma_y^2}, \varepsilon_4 = 1 - \frac{8\sigma_{xy}^2}{\sigma_x^4 + \sigma_y^4 + 2\sigma_{xy}^2},$$

where  $\sigma_x$  and  $\sigma_y$  are the respective root-mean-square widths of the density distributions and  $\sigma_{xy} = \overline{xy} - \bar{x}\bar{y}$ ; here, bars denote a convolution with the density distribution for a given configuration and averaging is performed over configurations. This procedure ensures that the fluctuation in the orientation of the initial almond-shaped collision zone is taken into account [26, 27]. For the Glauber calculations, the initial entropy profile in the transverse plane was assumed to be proportional to a linear combination of the number density of participants and binary collisions [29]. This assures that the entropy density weighting is constrained by multiplicity measurements.

The eccentricity scaled  $v_2$  and  $v_4$  values obtained with fKLN eccentricities, are shown in Fig. 3. For the lowest  $p_T$  selection, they indicate relatively small scaling violations. However, these violations progressively increase as the  $p_T$  for charged hadrons is increased. That is, the data points slope progressively upward (from low to high  $N_{\text{part}}$ ) as the magnitude of the  $p_T$  selection is increased. Relative to mid-central events, a large scaling violation of  $\frac{v_4}{\varepsilon_4}$  is also apparent for the two most central bins ie. for  $N_{\text{part}} > 250$ . We have traced this to a small overestimate of fluctuations which only impacts the value of  $\varepsilon_4$  in the most central collisions as illustrated by the gray diamonds in Fig. 3. The latter shows the resulting values of  $\frac{v_4}{\varepsilon_4}$  when an attempt is made to account for the overestimate by introducing a very small correlation between the  $\varepsilon_2$  and  $\varepsilon_4$  axes.

A similar scaling test was performed with the Glauber model eccentricities. The resulting  $\frac{v_2}{\varepsilon_2}$  and  $\frac{v_4}{\varepsilon_4}$  values vs.  $N_{\text{part}}$ , show trends which are relatively similar to the ones exhibited in Fig. 3, albeit with somewhat larger scaling violations. However, as discussed below, our fitting procedure provides a good constraint for choosing between the fKLN and Glauber model eccentricities.

#### 4.2. Estimation of the degree of local equilibrium, $\frac{\eta}{s}$ and $\lambda$

As discussed earlier, the quantification of scaling violations is an important step for reliable estimates of  $\frac{\eta}{s}$ ,  $\lambda$  and the degree of local equilibrium. This has been accomplished by performing simultaneous fits to the eccentricity-scaled  $v_2$  and  $v_4$  data for each of the  $p_T$  selections. For these fits, we follow the same fitting ansatz proofed in section 3, ie. we use Eq. 2;

$$\frac{v_{2k}}{\varepsilon_{2k}} = \frac{v_{2k}^h}{\varepsilon_{2k}} \left[ \frac{K^{-1}}{K^{-1} + K_0^{-1}} \right]^k \quad k = 1, 2 \quad \text{and} \quad K^{-1} = \beta N_{\text{part}}^{1/3}.$$

Here again, the scaled hydrodynamic limits  $\frac{v_{2k}^h}{\varepsilon_{2k}}$ , and  $\beta$  are fit parameters. Note as well that  $\beta$  allows the extraction of  $K$  values as a function of  $N_{\text{part}}$ , for each fit.

The requirement of a simultaneous fit to the eccentricity-scaled data ensures that the same  $K$  values are extracted from the  $v_2$  and  $v_4$  measurements. Equally important is the fact that they provide a constraint for making a choice between the fKLN and Glauber eccentricities. That is, Glauber eccentricities result in relatively poor simultaneous fits while the fKLN eccentricities give very good simultaneous fits ( $R_{\text{adj}}^2 \sim 1$ ) as shown by the dotted curves in Fig. 3. These fits underscores the fact that data comparisons for different centralities, as well as ratios such as  $\frac{v_4}{(v_2)^2}$  must take account of eccentricity differences.

As pointed out earlier, each fit gives a value for the hydrodynamic limits  $\frac{v_2^h}{\varepsilon_2}$  and  $\frac{v_4^h}{\varepsilon_4}$ , and a  $\beta$  value which determines  $K$  as a function of  $N_{\text{part}}$ . With these  $K$  values, the degree of local equilibrium and  $\frac{\eta}{s}$  can be estimated using Eqs. 2 and 3 respectively. To estimate  $\frac{\eta}{s}$  at a given centrality, we assume a temperature



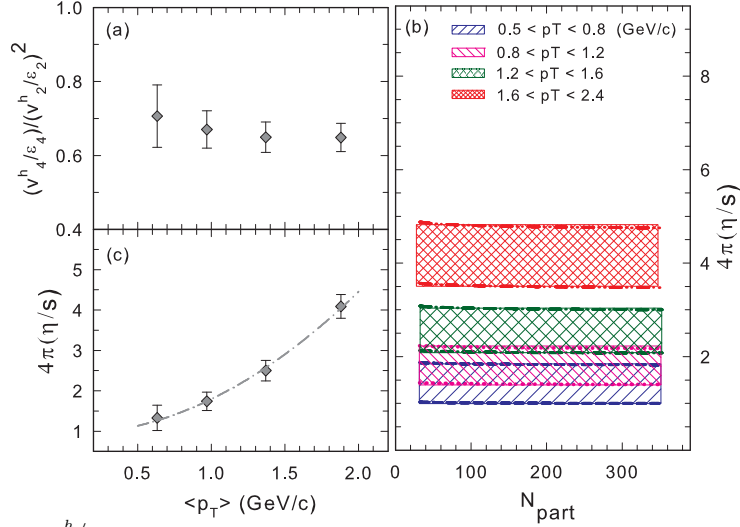


**Fig. 4.** (a)  $\frac{v_4^h/\varepsilon_4}{(v_2^h/\varepsilon_2)^2}$  vs.  $p_T$ , see text; (b) extracted bands for  $4\pi(\eta/s)$  vs.  $N_{\text{part}}$  for several  $p_T$  selections as indicated; (c) extracted values of  $4\pi(\eta/s)$  vs.  $p_T$ .

$T = 220 \pm 20$  MeV [ 30] for the plasma when flow develops<sup>2</sup>, and use the the lattice EOS to estimate the associated value of  $c_s = 0.47 \pm 0.03$  c. For any given centrality,  $\lambda = \bar{R}K$  is evaluated with the aid of the calculated transverse size  $\bar{R}$ , obtained for that centrality.

Figure 4 summarize the main results from our extractions with the fKLN eccentricities. It is noteworthy that the trends of the results obtained with the Glauber model eccentricities are essentially the same, albeit with different magnitudes. Panel (a) shows that, within errors, the ratio of the extracted hydrodynamic limits  $\frac{(v_4^h/\varepsilon_4)}{(v_2^h/\varepsilon_2)^2}$  change little, if any, with hadron  $\langle p_T \rangle$ . The extracted bands for  $4\pi(\eta/s)$  are shown as a function of  $N_{\text{part}}$  in Fig. 4(b). The essentially flat dependence on  $N_{\text{part}}$  demonstrates the important role of the transverse size and the eccentricity of the collision zone. It further suggests that even though  $K$  increases as collisions become more peripheral,  $\lambda$  does not have a strong dependence on collision centrality.

In contrast to the  $N_{\text{part}}$  dependence, Fig. 4(b) implies a relatively strong  $p_T$  dependence for the extracted  $4\pi(\eta/s)$  values, ie.  $\eta/s$  increases by almost a factor of four over the indicated  $p_T$  range. This  $p_T$  dependence is made more transparent in Fig. 4(c) where we plot  $4\pi(\eta/s)$  vs. the mean value of the  $p_T$  ranges indicated in Fig. 4(b). The dashed-dot curve in the figure illustrates the quadratic nature of this  $p_T$  dependence. Here, we wish to emphasize that this quadratic dependence on

<sup>2</sup>A centrality dependent  $T$  would results in an additional uncertainty on the extracted  $\frac{\eta}{s}$  values.

$p_T$  is **not** related to an intrinsic property of the QGP. Instead, it reflects the finding by Teaney [31] that viscous corrections to ideal hydrodynamics grow as

$$\left(\frac{p_T}{T}\right)^2 K.$$

Since our extracted  $K$  values include the  $p_T$ -dependent factor given in the above expression, they give rise to the quadratic  $p_T$  dependence of  $4\pi(\eta/s)$  observed in Figs. 4(b) and (c). This also indicates that a  $p_T$ -independent estimate of  $4\pi(\eta/s)$  is obtained when the magnitude of  $p_T \approx T$ .

The slow rate of increase of  $4\pi(\eta/s)$  at low  $p_T$  (cf. Fig. 4(c)) allows the use of the results for lowest  $p_T$  hadrons to constrain the estimates  $4\pi(\eta/s) = 1.3 \pm 0.3$  and  $\lambda = 0.25 - 0.3$  fm for the plasma. The corresponding estimate for the degree of local equilibrium is within 5 - 10% of the value for a system having an  $\frac{\eta}{s}$  value equal to the conjectured lower bound of  $\frac{1}{4\pi}$ . To estimate the latter, we use the  $K$  values extracted from the fit to the simulated data (for  $4\pi(\eta/s) = 1$ ) shown in Fig. 1. Our  $\eta/s$  estimate is in good agreement with prior extractions [4, 5, 6, 15, 32, 33]. Our  $\lambda$  estimate also indicates that the low  $\eta/s$  value is associated with a relatively short mean free path in the plasma. We interpret these observations as an important indication for a strongly coupled QGP.

## 5. Conclusions

To conclude, we have made detailed studies of possible hydrodynamic scaling violations of the eccentricity scaled  $v_4$  and  $v_2$  flow coefficients for charged hadrons. These studies validate the hydrodynamic scaling patterns expected for a nearly inviscid system close to thermal equilibrium i.e. only 5-10% less than the value estimated for a system having an  $\eta/s$  value equal to the conjectured lower bound of  $1/4\pi$ . They also provide the estimates  $4\pi(\eta/s) = 1.3 \pm 0.3$  and  $\lambda = 0.25 - 0.3$  fm. These estimates suggest that the transverse expansion dynamics leading to anisotropic flow favor the creation of a strongly coupled QGP in collision zones for central and mid-central Au+Au collisions at  $\sqrt{s_{NN}} = 200$  GeV.

## Acknowledgments

This work was supported by the US DOE under contract DE-FG02-87ER40331.A008.

- a.* Permanent address: Chemistry Dept., Stony Brook University, Stony Brook, USA;  
E-mail: Roy.Lacey@Stonybrook.edu

## References

1. A. Adare et al., *Phys. Rev. Lett.* **98** (2007) 162301.

2. R. A. Lacey and A. Taranenko, *PoS CFRNC2006* (2006) 021.
3. U. Heinz and P. Kolb, *Nucl. Phys.* **A702** (2002) 269.
4. E. Shuryak, *Prog. Part. Nucl. Phys.* **62** (2009) 48.
5. P. Romatschke and U. Romatschke, *Phys. Rev. Lett.* **99** (2007) 172301.
6. Z. Xu, C. Greiner and H. Stoecker, *Phys. Rev. Lett.* **101** (2008) 082302.
7. N. Borghini and J.-Y. Ollitrault, *Phys. Lett.* **B642** (2006) 227.
8. M. Asakawa, S. A. Bass and B. Muller, *Phys. Rev. Lett.* **96** (2006) 252301.
9. E. Glass Gold et al., *Annals of Physics* **6** (1959) 1.
10. G. Chapline, M. Johnson, E. Teller and M. Weis, *PRD* **8** (1973) 4302.
11. W. Scheid, H. Muller and W. Greiner, *PRL* **32** (1974) 741.
12. H. Stoecker, J. Maruhn and W. Greiner, *PRL* **44** (1980) 725.
13. T. Schaefer and D. Teaney (2009).
14. R. S. Bhalerao et al., *Phys. Lett.* **B627** (2005) 49.
15. H.-J. Drescher, A. Dumitru, C. Gombeaud and J.-Y. Ollitrault, *Phys. Rev.* **C76** (2007) 024905.
16. C. Gombeaud and J. Y. Ollitrault, *Phys. Rev.* C77, 054904, 2008; and private communication.
17. C. Marle, *Annales Poincare Phys. Theor.* **10** (1969) 67.
18. H. Song and U. W. Heinz, *Phys. Rev.* **C78** (2008) 024902.
19. M. Knudsen, *Ann. Phys. (Leipzig)* **28** (1909) 75.
20. P. Danielewicz and M. Gyulassy, *Phys. Rev.* **D31** (1985) 53.
21. P. Kovtun, D. T. Son and A. O. Starinets, *Phys. Rev. Lett.* **94** (2005) 111601.
22. D. Kharzeev and E. Levin, *Phys. Lett.* **B523** (2001) 79.
23. S. S. Adler et al., *Phys. Rev. Lett.* **91** (2003) 182301.
24. A. M. Poskanzer and S. A. Voloshin, *Phys. Rev.* **C58** (1998) 1671.
25. J. Jia, *Nucl. Phys.* **A783** (2007) 501.
26. M. L. Miller, K. Reygers, S. J. Sanders and P. Steinberg, *Ann. Rev. Nucl. Part. Sci.* **57** (2007) 205.
27. B. Alver et al., *Phys. Rev. Lett.* **98** (2007) 242302.
28. H.-J. Drescher and Y. Nara, *Phys. Rev.* **C76** (2007) 041903.
29. T. Hirano and Y. Nara (2009).
30. A. Adare et al. (2008).
31. D. Teaney, *Phys. Rev.* **C68** (2003) 034913.
32. R. A. Lacey et al., *Phys. Rev. Lett.* **98** (2007) 092301.
33. A. Adare et al., *Phys. Rev. Lett.* **98** (2007) 172301.